

# Time resolved measurements of the flow generated by suction feeding fish

Steven W. Day  Timothy E. Higham   
Peter C. Wainwright

Received: 20 February 2007 / Revised: 25 August 2007 / Accepted: 15 September 2007 / Published online: 12 October 2007  
Springer-Verlag 2007

**Abstract** The majority of aquatic vertebrates are suction feeders: by rapidly expanding the mouth cavity they generate a fluid flow outside of their head in order to draw prey into their mouth. In addition to the biological relevance, the generated flow field is interesting fluid mechanically as it incorporates high velocities, is localized in front of the mouth, and is unsteady, typically lasting between 10 and 50 ms. Using manometry and high-speed particle image velocimetry, this is the first study to quantify pressure along as the unsteady nature of the flow is included. Measurements with a high temporal (2 ms) and spatial (1 mm) resolution were made for several feeding events of a single largemouth bass (*Micropterus salmoides*). General properties of the flow were evaluated, including the transient velocity field, its relationship to a flow of water outside the head that acts to draw the prey pressure within the mouth and pressure at the prey. We find that throughout the feeding event a relationship exists for the magnitude of fluid speed as a function of distance from the predator mouth that is based on scaling the velocity field according to the size of the mouth opening and the time lasting

locomotion through a fluid medium, feeding involves some direct fluid-structure interactions. Forces are a function of the biomechanical forces within the fish and the fluid mechanical pressure within mouth. The speed of cranial expansion is a function of the biomechanical kinematics within the animal and also the volumetric flow rate of the fluid. Force and speed of fish movement are related through muscle physiology and gearing within the animal, and pressure and fluid speed are related through the governing equations of fluid mechanics. As an example, an attempt by a fish to increase the speed of mouth opening increases the required force through interaction of the fluid field; increased fluid speeds lead to increased magnitude of generated pressures.

---

S. W. Day (✉)  
Department of Mechanical Engineering,  
Rochester Institute of Technology,  
76 Lomb Memorial Dr, Rochester, NY 14623, USA  
e-mail: steven.day@rit.edu

T. E. Higham  
Department of Organismic and Evolutionary Biology,  
Concord Field Station, Harvard University,  
100 Old Causeway Road, Bedford, MA 01730, USA

P. C. Wainwright  
Section of Evolution and Ecology,  
University of California, One Shields Avenue,  
Davis, CA 95616, USA

Species of fish exhibit variations in suction feeding within the flow field and would be present even in the behavior, including some with relatively large mouths that lack the velocity field in front of a fish's mouth. While the characteristics of the swim rapidly towards the prey when feeding and some that have small mouths and hold their body still while drawing the prey into the mouth, as have been investigated by Norton and Brainerd (1993), Norton (1991), and Higham et al. (2007). Individuals within a given species can modulate aspects of this feeding behavior with muscular control, including the speed with which they open the mouth and the maximum size of the mouth opening. For example, Nemethy (1997) demonstrated that more aggressive feedings (i.e. faster mouth opening) are employed when feeding on more evasive prey. Extensive research by Aerts et al. (1987), Aerts (1990), Lauder (1980), Liem (1973), Carroll et al. (2004), and Svanback et al. (2002) has investigated the musculoskeletal basis of suction feeding. van Wassenbergh et al. (2006) have devoted some attention to the study of the generated flow.

Initial investigations into the fluid mechanics of suction feeding based on mathematical models using potential flow theory include those by Drost et al. (1988), Muller et al. (1982), Weihs (1980) and van Leeuwen and Muller (1984). Earlier empirical studies included qualitative visualization by Muller and Ossinger (1984), van Leeuwen and Muller (1984) and quantitative measurements of speed by particle streaking at a few locations in front of the fish (Lauder and Clark 1984). Recent studies by our group, including Day et al. (2005) and Higham et al. (2006a) used particle image velocimetry (PIV) to resolve the flow field in front of two species of fish with sufficient spatial and temporal resolution to quantify the distribution of fluid speed as a function of distance in front of the fish and investigated the effect of swimming speed (or speed), mouth size, and time of mouth expansion on the effect of substrate on water flow patterns generated by sharks.

This flow field as described by distributions of velocity and pressure is central to the suction feeding event because it imparts all of the forces that act to draw the prey into the predator's mouth. The traditional view is that pressure within the mouth drives the velocity field and the forces imparted onto the prey are caused by drag and acceleration reaction force, both of which are a consequence of the generated velocity field. Recently, Wainwright and Day (2007) proposed that there are three forces that the flow can exert onto a prey item: drag and the acceleration reaction are caused by the relative motion of the fluid and prey, both of which are a result of the velocity field. The pressure gradient force (Batchelor 1967) is, however, a direct result of gradients of pressure

study we couple manometry with the PIV method used in prior studies in order to empirically determine the temporal relationship between the velocity field in front of suction feeding largemouth bass and pressure at two critical locations, within the mouth and at the prey. We demonstrate that, while substantial fluid velocities are confined to a region near the mouth of the fish, the sub-ambient pressures extend an even smaller distance into the flow. We describe the temporal patterns of velocity and pressure and demonstrate directly that maximum sub-ambient pressure occurs before peak fluid speeds. We show that, although the velocity field varies with time, the distribution of fluid power in front of the fish is still a function of only the instantaneous gape and fluid speed at the mouth. We are able to demonstrate the effectiveness of applying the momentum equation to predict the relationship between the generated velocity field outside the mouth and pressure within the mouth and to demonstrate the contribution of the fluid momentum to pressure within the mouth.

that, while substantial fluid velocities are confined to a region near the mouth of the fish, the sub-ambient pressures extend an even smaller distance into the flow. We describe the temporal patterns of velocity and pressure and demonstrate directly that maximum sub-ambient pressure

occur before peak fluid speeds. We show that, although the velocity field varies with time, the distribution of fluid power in front of the fish is still a function of only the instantaneous gape and fluid speed at the mouth. We are able to demonstrate the effectiveness of applying the momentum equation to predict the relationship between the generated velocity field outside the mouth and pressure within the mouth and to demonstrate the contribution of the fluid momentum to pressure within the mouth.

## 2 Materials and methods

### 2.1 Experimental animals

One largemouth bass (*Micropterus salmoides* Rafinesque, with a standard length of 18.5 cm) was used in this study. The fish was caught in Yolo County, near Davis, CA and housed in a 100 l aquarium. The fish was fed a variety of squid (*Loligo*) and live ghost shrimp (*Palaemonetes*) daily. All fish maintenance and experimental procedures used in this research followed a protocol approved by the University of California, Davis Animal Care and Use Committee. Six feeding sequences were analyzed for this individual. The low inter-individual variance with respect to fluid speed–pressure relationships found in a previous study using this species (Higham et al. 2006b) suggests that using a single individual is a valid approach for measuring the relationship between the fluid velocity field in front of the feeding fish and pressures within the mouth. All values are reported as the mean  $\pm$  standard deviation for these six feedings.

### 2.2 Experimental setup

Experiments were conducted in a 200 l experimental aquarium that was integrated with a PIV system. Digital particle image velocimetry (DPIV) is a well-established technique (Adrian 1991) that measures the nearly instantaneous velocity field within an illuminated plane of the fluid field using light scattered from particles seeded into the fluid. This method is very versatile and ideally suited

for non-uniform transient flows. Similarly, miniature pressure transducers developed for blood vessel catheterization are commercially available. Details of both the PIV and the manometry system used in these experiments follow.

### 2.2.1 Particle image velocimetry

The illumination used in this experiment consists of an Hanovia I-90 continuous argon-ion laser with an output power of  $\approx 3$  W (Coherent, Inc., Santa Clara, CA, USA). A matched set of a single cylindrical and spherical lens created a collimated light sheet about 10 cm wide and was focused to a waist thickness of approximately 1 mm within the measurement region. The laser sheet was directed upwards by a mirror located below the tank and passed into the aquarium through the tank bottom (Fig. 1). The

resulting sheet was parallel to the sagittal plane (plane of symmetry) of an approaching fish. After traversing the depth of the tank, a mirror near the surface of the tank reflected the laser sheet back down within the same plane as the upward directed sheet, but angled towards the posterior of the fish. In this experiment, the downward directed sheet illuminated the fluid field above the upper lip of the fish that was in the shadow of the upward directed beam, but the methods may be useful for illuminating the flow in the shadow of any opaque object. Additionally, most of the flow field is illuminated by both the “upward” and the “reflected” sheets, thereby nearly doubling the amount of scattered light.

The seed particles used for light scattering were nominally  $14\ \mu\text{m}$  silver-coated glass beads manufactured for light scattering in reflective paints (Potter Industries, Inc., Carlstadt, NJ). The particles are hollow and have an

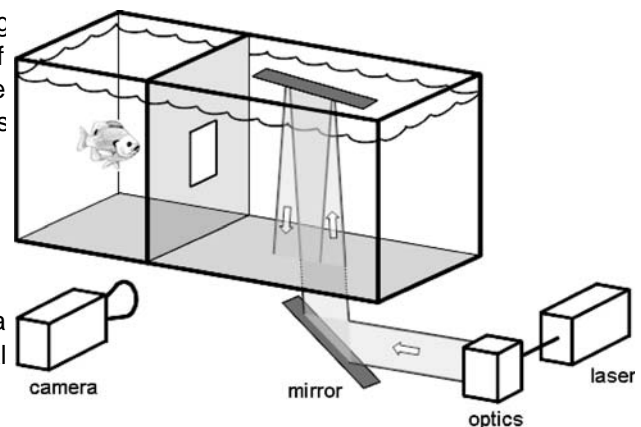


Fig. 1 Schematic of the experimental setup, showing experimental tank, position of laser sheet, optics, mirrors, camera, fish prior to a feeding, tank divider and door

average specific gravity of approximately 1.05 which, when used in fresh water, results in a calculated settling velocity of  $5 \times 10^{-4}$  mm/s (Durrani and Greathead 1977). In practice, it was apparent that a fraction of the particles settled out of the flow within 10–15 min, so we suspect that the density of the particles is variable.

The scattered light was imaged and collected by a NA Memrecam ci digital high-speed video camera (Tokyo, Japan) through an f/1.2 c-mount video lens. The Memrecam ci is a high speed CMOS based camera with full resolution (512 × 462 pixels) at 500 frames per second. As the laser was not shuttered or pulsed, a mechanical shutter that is built into the camera was used to give an exposure time of 1/3,000 s. This was sufficiently short to prevent blurring and long enough to provide adequate signal (\* 1 mJ/image).

## 2.2.2 Manometry

Two pressure transducers were used in these experiments. The first, hereafter referred to as  $p_{\text{mouth}}$ , was surgically implanted into the fish skull. The second, referred to as  $p_{\text{prey}}$ , was attached to the prey mount and so moved with the prey up until the point of ingestion. Typically, as the prey moved into the mouth aperture, the prey mount contacted the upper lip of the fish so that the mount and transducer remained in the mouth aperture (see Fig. 1).

In order to implant the mouth transducer, the fish was anesthetized by submerging it in a 0.3% solution of buffered MS-222 (Carroll et al. 2004). Once anesthetized, as determined by a cessation of gill ventilation and lack of response to tactile stimulation, the fish was positioned

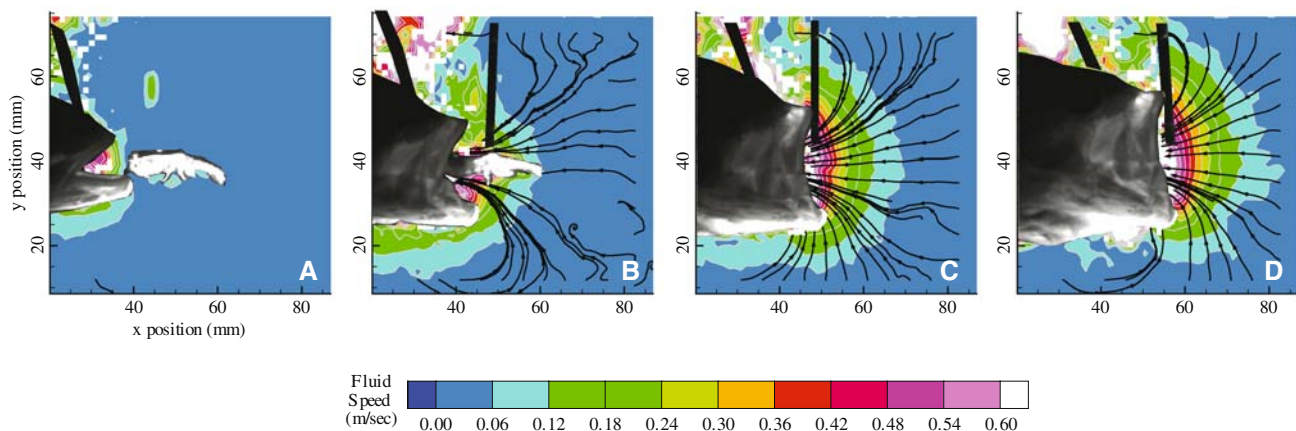


Fig. 2 PIV measurements in front of a bass feeding on a live, mounted ghost shrimp at four instants during the feeding. Times are measured from the time that mouth opening began, the time of each measurement is clear as a black object protruding from the mouth. The position of the predator and the fish head. A second cannula that houses the pressure transducer prey are both shown as overlays onto the calculated velocity field located at the prey is also seen in the image

response of 10 kHz. Pressure transducers were calibrated prior to the surgery by placing them into a sealed flask. The pressure within the flask was varied over a range of 0–60 kPa using a vacuum pump and was measured with a commercial (World Precision Instruments, Sarasota, FL, USA) pressure transducer that came with an NIST certificate of calibration. The voltage output of the transducer is a linear function of pressure ( $r^2 = 0.99$ ).

The transducer at the prey was housed in and protected by a short length of stainless steel tubing in order to both

maintain the position of the transducer and to protect it when contacted by the feeding Psh. The tubing was attached with glue and thread to the prey mount, so that the open and exposed end of the housing was just above the prey. Thin plastic tubing (PE-90) connected the top of the stainless tubing to a syringe located outside the tank. This was used to purge the cannula before each feeding.

The output of the mouth and prey pressure transducers were sent to linear op-amp based amplifiers with gains of 10 and 25 respectively. The amplified voltages were on the order of 1 V and were recorded at a sampling rate of 5 kHz using a National Instruments analog to digital converter (ADC) and LabView software (DAQPad-6070E National Instruments, Austin, Texas). Since the baseline pressure was varied depending on the depth of the Psh, we refer to instantaneous pressure and the baseline value prior to the feeding event. Both the camera and ADC have a circular buffer, so that when armed they are continually acquiring data until triggered. In these experiments the pressure and video recordings were synchronized by using an external manual button to trigger both devices.

### 2.3 Experimental protocol

The Psh was easily trained over the course of several days to reliably feed within the laser sheet. Prior to beginning the experiment, the Psh was confined to one end of the tank by a physical barrier. The prey was suspended and positioned in the laser sheet and the camera field of view by a flexible (0.15 in. diameter) wire inserted under the exoskeleton, so that the shrimp generally remained alive and initiated an escape in response to the approaching predator. To keep the predator motivated, unrestrained prey were occasionally introduced during feeding sessions. The Psh was confined to one end of the tank until a trap door was reopened at the beginning of each experiment (Fig. 1). The Psh swam through the door and towards the prey, suspended in the measurement region. The Psh's movements were not confined in any direction, but due to the relative location of the trap door and prey, generally swam downwards

Determining the uncertainty of correlation-based PIV methods complicated, but well studied. Generally, uncertainty increases as a result of poor seeding in that region of the image, high velocity gradients, solid boundaries that scatter light, and particle displacements that are large relative to the size of the interrogation region, as is described by Adrian (1997). The following two-step validation scheme was implemented.

First, vectors with a signal-to-noise ratio (SNR) of less than 2.0 were removed, without replacement, and no

smoothing was applied to the PIV velocity field. Some value, respectively. The time between these is referred to as spurious measurements that are not representative of fluid particle displacement still passed the SNR validation criterion. The second step of the validation scheme deals with these spurious vectors. For velocities extracted from a transect extending away from the mouth along the centerline of the Psh, measurements both directly on the transect at  $(i, j)$  and at 2 grid points above  $(i + 2, j)$  and 2 grid points below  $(i, j - 2)$  were considered at each horizontal position. Measurements located 2 grid points away from the primary measurement location are used because these do not overlap the primary measurement region. The neighboring points in the direction were not used for validation because of the very steep gradients of fluid velocity in the horizontal direction. If at least two of the three measurements considered had not been removed based on the SNR criterion (step one of the validation scheme), then the mean of the remaining measurements was used as the value of the speed for that given position along the transect.

This validation scheme resulted in the removal of some measurements near the mouth for all sequences. Measurements near the mouth were the most likely to fail the validation scheme because particle displacements (high fluid speed), velocity gradients, and occasional glare from the predator were all highest in this region. The camera

frame rate and spatial resolution used for the measurements placed an effective upper bound of measured fluid speed at approximately 1.5 m/s, corresponding to 16 pixel displacement between images. For the majority of feedings, all measurements greater than 2–3 mm from the mouth and passed the validation procedure and measurements further than 5 mm from the mouth were validated for all feedings.

### 2.3.2 Data analysis

The position of the eye and upper and lower jaws were manually identified and measured for each frame of the acquired video sequence using Image J (NIH, Washington, DC, USA). The  $x, y$  position of each was used to calculate the position of the center of the mouth was defined as the midpoint between the upper and lower jaw tips. Gape was the distance from tip of the upper jaw to tip of the lower jaw and Peak Gape (PG) was the maximum value of gape during the feeding. Ram speed was calculated as the horizontal component of the temporal derivative of eye position. The measurements of horizontal position were smoothed with a three-point moving average before calculating derivative quantities. The onset of mouth opening and the onset of peak gape are defined as the time at which the mouth has opened to 20 and 95% of its maximum

the pressure transducer located at the prey mouth placed an effective upper bound of measured fluid speed at approximately 1.5 m/s, corresponding to 16 pixel displacement between images. For the majority of feedings, all measurements greater than 2–3 mm from the mouth and passed the validation procedure and measurements further than 5 mm from the mouth were validated for all feedings. scaling of the velocity field, the acquired pressures at the prey are scaled. The magnitude of each measurement of pressure at the prey,  $p_{prey}$ , was divided by the instantaneous pressure in the Psh mouth,  $p_{mouth}$ , and the spatial position of each was divided by the instantaneous gape. This results in a distribution of scaled pressure as a function of non-dimensional position  $x^* = x/G$  in front of the mouth. It should be remembered that the profile of pressure versus distance was not acquired at a single instantaneous time for each feeding, but is the compilation of single point measurements taken over the period of the feeding. Nonetheless, each is scaled by the instantaneous pressure in the Psh mouth and instantaneous gape. Finally, the measured distribution of the velocity in front of the Psh was used to calculate a predicted pressure within the buccal cavity according to the momentum equation along the centerline of the Psh. We integrated the differential form of one-component of the momentum equation (Eq. 1) along a path extending from a point far away from the Psh and ending at the mouth aperture in order to find the relationship between  $p_{mouth}$  and  $p_{ambient}$  (Eq. 2).

$$\frac{dp}{dx} = -\rho \left( \frac{\partial u}{\partial t} + u \frac{\partial u}{\partial x} \right) \tag{1}$$

$$p_{\text{mouth}} - p_{\text{ambient}} = \int_{x_{\text{ambient}}}^{x_{\text{mouth}}} \frac{dp}{dx} dx = \int_{x_{\text{ambient}}}^{x_{\text{mouth}}} \rho \left( \frac{\partial u}{\partial t} + u \frac{\partial u}{\partial x} \right) dx \tag{2}$$

Implementation of the momentum equation directly on the raw PIV data leads to high uncertainty because of the derivative terms, so we instead fit a function to the empirical data and then applied the equation to this function. The spatial distribution of fluid speed is specified by a polynomial fit to the empirical data. The curve-fit for the time course of fluid speed is based on the form of equation 11 from Muller et al. (1982) with parameters manually adjusted to agree with the empirical data for that particular feeding. This implementation resulted in a function of predicted pressure at the mouth aperture that was arrived independently of the measured  $p_{\text{mouth}}$ . This predicted pressure was compared to the measured  $p_{\text{mouth}}$  in order to validate the utility of this relationship.

### 3 Results

The suction feeder creates a velocity and pressure field that both have high spatial and temporal gradients. Speeds are highest near the mouth ( $1.5 \pm 0.36$  m/s) and decrease as a function of distance away from the mouth. There is a general shape of contour lines of constant velocity throughout the feeding that we describe as the top of a mushroom (Fig 2). This pattern is symmetric about the long-axis of the  $\beta$ sh. The size of the pattern varies in proportion to the diameter of the mouth and the magnitude of velocity at the mouth varies throughout the feeding. Both the size of the affected region and magnitude of fluid speed are highest at a time shortly after reaching peak gape. The  $\beta$ sh continues to ingest water throughout the duration of the feeding, even as the mouth is closing, as shown in Figs. 2 and 3.

#### 3.1 Temporal pattern

There is a general temporal pattern of generated fluid speed at peak gape, and the recorded pressures (see Fig 3 for a representative sequence). All times are given as both the absolute time (relative to the beginning of mouth opening) and as a fraction of TTPG, the time between beginning of mouth opening and peak gape, as the relative timing of events scales in proportion of the total duration of the feeding. Maximum sub-ambient pressure in the mouth ( $-5.7 \pm 1.9$  kPa) occurs

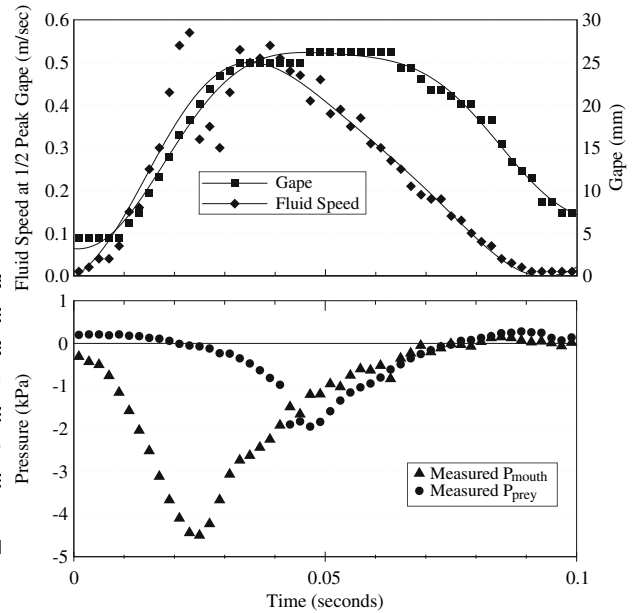


Fig. 3 Relative time course of fluid speed compared to gape distance and pressures within and outside the mouth for the representative sequences. Fluid speed is measured at a constant distance in front of the  $\beta$ sh equal to 1/2PG. This is a moderate speed feeding (time to open mouth\* 25 ms). The relative timing of events is similar for all recorded feedings. Peak fluid speed occurs slightly before the onset of peak gape. The pressure within the mouth reaches its maximum sub-ambient pressure during mouth opening and has already decayed significantly by the time of mouth opening. The pressure at the prey,  $p_{\text{mouth}}$  is near ambient, but gradually decreases as both fluid speed increase and the prey moves closer to the predator's mouth. Near 48 ms, the prey enters the mouth. The transducer and mouth are in contact with the upper lip of the  $\beta$ sh, so the transducer remains in the aperture until the end of the feeding. During this time, the pressure measured near the mouth aperture and within the buccal cavity are nearly equal. At a time ( $24 \pm 18$  ms,  $58 \pm 18\%$  TTPG) when the mouth is still opening and has typically decayed to approximately 1/2 the peak amplitude at the onset of peak gape ( $38 \pm 21$  ms,  $100 \pm 0\%$  TTPG), consistent with Sanford and Wainwright (2002). Peak fluid speed ( $1.50 \pm 0.36$  m/s) reached a maximum just after ( $38.3 \pm 20.3$  ms,  $113 \pm 41\%$  TTPG) the onset of peak gape, consistent with Day et al. (2005) and Higham et al. (2006a). Peak gape is maintained for some time ( $25 \pm 9.7$  ms) before the mouth begins to close. At the end of peak gape ( $0.63 \pm 0.20$  m/s), as indicated by the mouth diameter having reached its maximum and then decreased to 65% of its maximum size, fluid speed at the mouth has decreased to a fraction ( $32 \pm 28\%$ ) of the maximum speed for that feeding. The pressure at the prey is initially very small and decreases exponentially as a result of both the flow speed increasing and the prey moving towards the mouth. At the time when the prey is at the mouth opening (48 ms in this case), the pressure transducer is located in the mouth aperture and remains there for the duration of the feeding

after the prey is drawn off the wire and ingested. The transducer located at the prey,  $p_{prey}$ , records a nearly identical pressure as  $p_{mouth}$ . It should be emphasized that for all feedings that we recorded, the second transducer,  $p_{prey}$ , is located at the aperture only after peak gape and not during mouth expansion.

### 3.2 Spatial pattern

After creating a non-dimensional distance  $x^*$  (and speed (SS, scaled speed) by dividing all measured distances (by the instantaneous mouth diameter and dividing all fluid speeds (FS) by the fluid speed at a reference location located at a distance  $1/2$  of gape ( $x^* = 1/2$ ) in front of the  $\beta$ sh ( $FS_{1/2 \text{ gape}}$ ), the velocity profile along the centerline for all feedings collapse to one empirical relationship (Fig. Eq. 3). At all times during the feeding, fluid speed decays with distance in front of the feeding  $\beta$ sh, being equal to approximately 25% the speed at the mouth at a distance  $x^* = 1/2$  the mouth diameter and 5% at one mouth diameter in front of the  $\beta$ sh. Additionally, measurements from the pressure transducer located at the prey are presented. As the prey moved towards the predator during each feeding, the distance from mouth to prey was calculated and scaled by the instantaneous gape. The magnitude of pressure was scaled by the magnitude of measured pressure within the mouth cavity at that instant in time. Note that the decay of pressure in front of the  $\beta$ sh is even more dramatic than that of fluid velocity. There is a very steep pressure gradient very near the mouth and substantially less away from the mouth.

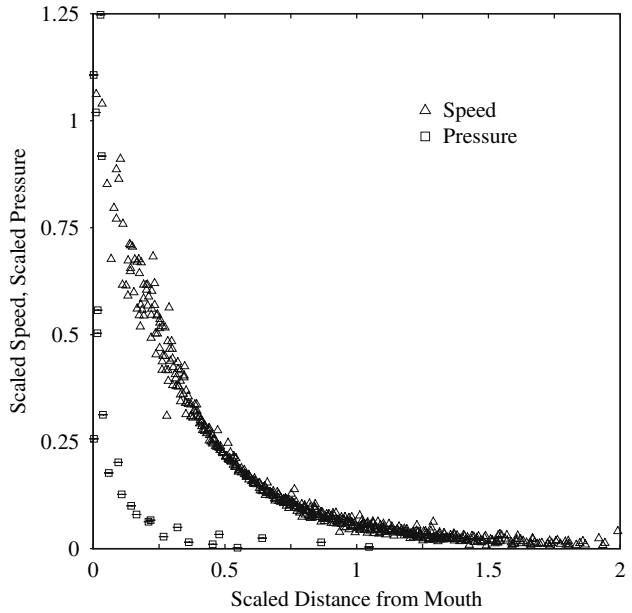


Fig. 4 Profiles of scaled speed and pressure along the centerline in front of the  $\beta$ sh. Additionally, measurements from the pressure transducer located at the prey are presented. As the prey moved towards the predator during each feeding, the distance from mouth to prey was calculated and scaled by the instantaneous gape. The magnitude of pressure was scaled by the magnitude of measured pressure within the mouth cavity at that instant in time. Note that the decay of pressure in front of the  $\beta$ sh is even more dramatic than that of fluid velocity. There is a very steep pressure gradient very near the mouth and substantially less away from the mouth.

The feeding *Micropterus* can modulate both of these, so that there is significant feeding-to-feeding variation. A fourth order polynomial fit to the data assembled for all feedings is given as

$$FS(x^*) = FS_{mouth}(0.215x^{*4} - 1.26x^{*3} + 2.73x^{*2} - 2.63x^* + 1) \quad (3)$$

The magnitude of fluid speed and gape vary throughout the feeding. After normalization based on FS at the mouth and the mouth diameter, both measured as a function of time, transects of scaled speed in front of the  $\beta$ sh have a very similar shape at all times during the feeding (Fig. 4), suggesting that Eq. 3 is an appropriate description of the spatial pattern of the velocity throughout the feeding.

### 3.3 Pressure outside the mouth

For most feedings, the onset of mouth opening occurs when the prey is approximately one mouth diameter in front of the  $\beta$ sh and the prey enters the mouth of the  $\beta$ sh slightly before the onset of peak gape ( $40 \pm 16$  ms,  $58 \pm 18$  ms). This allows for measurements of the pressure in front of the  $\beta$ sh during this period as the transducer attached to the prey moved towards the mouth. The distribution of pressure decays even more dramatically than

velocity in front of the  $\beta$ sh (Fig. 4). The pressure is approximately 10% the pressure within the mouth at a distance of  $1/4$  gape, and 5% at  $1/2$  gape, thereby only influencing a region that is extremely local to the  $\beta$ sh mouth. The spatial gradient of pressure is steepest at the mouth aperture and very small at a distance more than  $1/4$  gape from the  $\beta$ sh.

### 3.4 Model results

The existence of a general form of the spatial pattern of fluid speed (Eq. 3) based on fluid speed at the mouth ( $FS_{mouth}$ ) and the mouth aperture ( $G$ ), allows a mathematical function for the spatio-temporal pattern of fluid speed in front of the  $\beta$ sh so long as  $FS_{mouth}$  and  $G$  are specified as a function of time. The resulting spatio-temporal pattern of fluid speed along a line extending away from the  $\beta$ sh is shown in Fig. 5 for a representative feeding. Predictions of the pressure within the mouth based on the solution of Eq. 2 both neglecting (steady form) and including (unsteady form) the temporal derivative of velocity are compared in Fig. 7 for this same representative

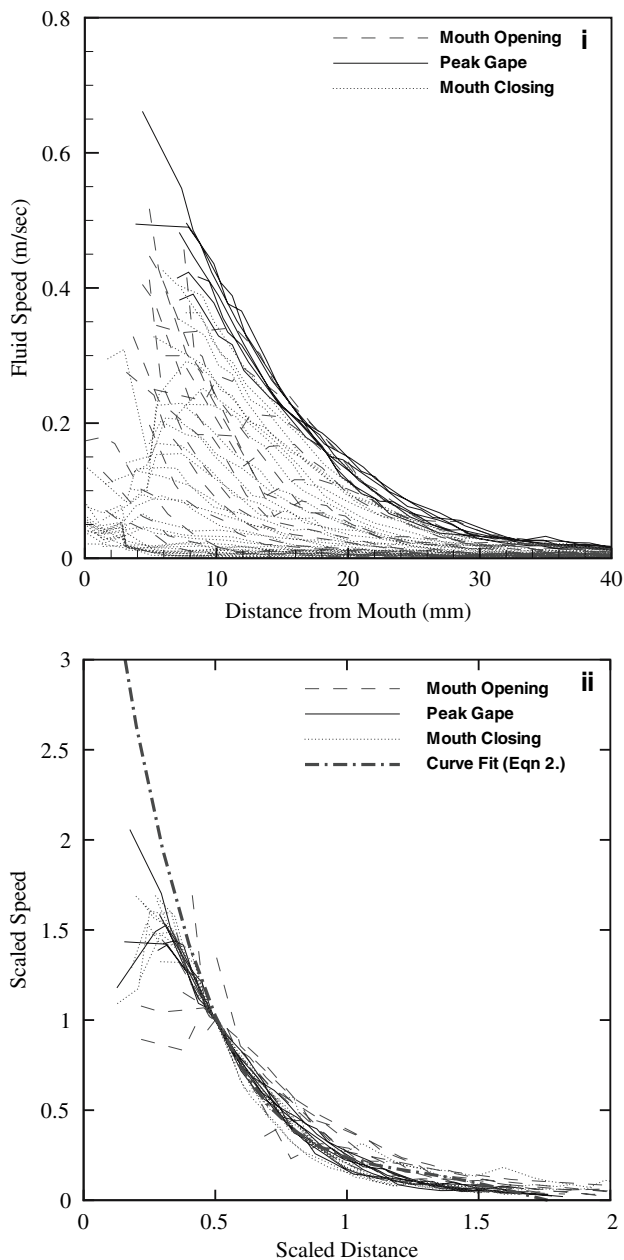


Fig. 5 Profiles of speed (a) and scaled speed (b) measured along the centerline at all times during the feeding, including mouth opening, the duration of peak gape and mouth closure. Both the magnitude and size of the velocity profile vary during the feeding. The same data as in a, but after scaling. The distance in front of the fish was scaled by the mouth diameter at the time of velocity measurement. Magnitudes of velocities were scaled by the FS measured at a distance of 1/2 gape at that time (FS<sub>1/2 gape</sub>). Variations in mouth size and the speed of flow at the mouth have a very significant effect on the absolute speeds in front of the fish, but the scaled profiles are similar at all times during the feeding

feeding. For all feedings, the time of peak sub-ambient pressure predicted based on the unsteady form of the model (25 ± 18 ms, 61 ± 19%TPG) agreed well with the empirical data (24 ± 18 ms, 58 ± 18%TPG), as shown in

Fig. 8. The steady form (30 ± 19 ms, 77 ± 21%TPG) predicted peak pressure to occur later than the unsteady form, and always after it was measured (Figs 8). The unsteady form predicts greater magnitude of sub-ambient pressures than the steady form (3.9 ± 1.1 kPa vs. 3.2 ± 1.0 kPa). For some feedings there is very good agreement between the magnitude of predicted and measured (5.7 ± 1.9 kPa) mouth pressures but the predicted pressure is smaller magnitude than the observed for most feedings (as is the case for the feeding shown in Fig. 9).

#### 4 Discussion

The simultaneous measurement of fluid speed and pressure presented here is one of the first empirical attempts to bridge the relationship between pressure and fluid speed in the complex, unsteady flow field that characterizes suction feeding. During suction feeding, the affected flow is confined to a region close to the mouth of the fish and the size of this region varies in direct proportion to mouth diameter throughout the feeding. The area of substantial fluid speed forms a three-dimensional shaped region similar to the top of a mushroom. This result is consistent with models by Muller and Osse (1984) and the empirical findings of Ferry-Graham et al (2003) and Day et al. (2005) for other species. This study also shows that the area of affected pressure is confined to an even smaller region than the area affected by the velocity field. The pressure gradient force, as opposed to velocity-based forces such as drag, has recently been proposed to be the dominant forces in many suction feeding scenarios by Wainwright and Day (2007). This study underscores the conclusion of previous studies that the predator must locate the prey in very close proximity to its mouth in order to have any effect on the prey.

Day et al. (2005) showed that a single polynomial fit to empirical data describes the distribution of fluid speed in front of the fish and showed that this relationship holds true at the time of peak fluid speed across a wide range of mouth size and fluid speed in a bluegill. Here we show that a similar polynomial function (Eq. 3) can be used to describe the spatial distribution of fluid speed at all times during the feeding for the largemouth bass. Velocity profiles scaled by the instantaneous gape and instantaneous fluid speed all fit one generalized function well. This result is consistent with previous findings that peak fluid speeds measured at three locations along the centerline transect all occurred nearly simultaneously with one another and with the onset of peak gape (95% opening) Higham et al. (2006). Further, this allows a description of the velocity field using only two parameters, the mouth diameter and fluid speed, which are specified as functions of time.

Fig. 6 Curve  $\beta t$  to the spatio-temporal pattern of fluid speed along the centerline transect in front of the feeding fish. Fluid speed in front of the fish is always given (Eq 3) as  $FS(x^*) = FS_{mouth} (0.215x^{*4} + 1.26x^{*3} + 2.73x^{*2} + 2.63x^* + 1)$ .  $FS_{mouth}$  is the fluid speed at the mouth (distance equals 0) and is specified as a function of time and is based on the form of equation 11 from Muller et al. (1982)

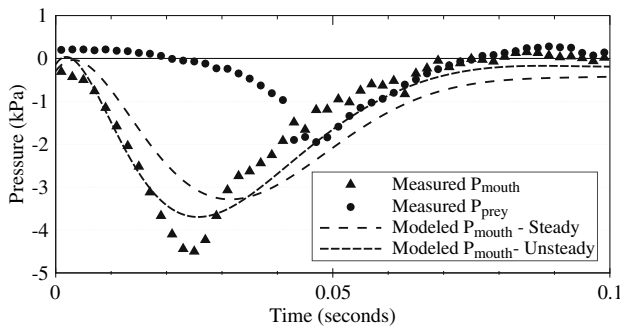
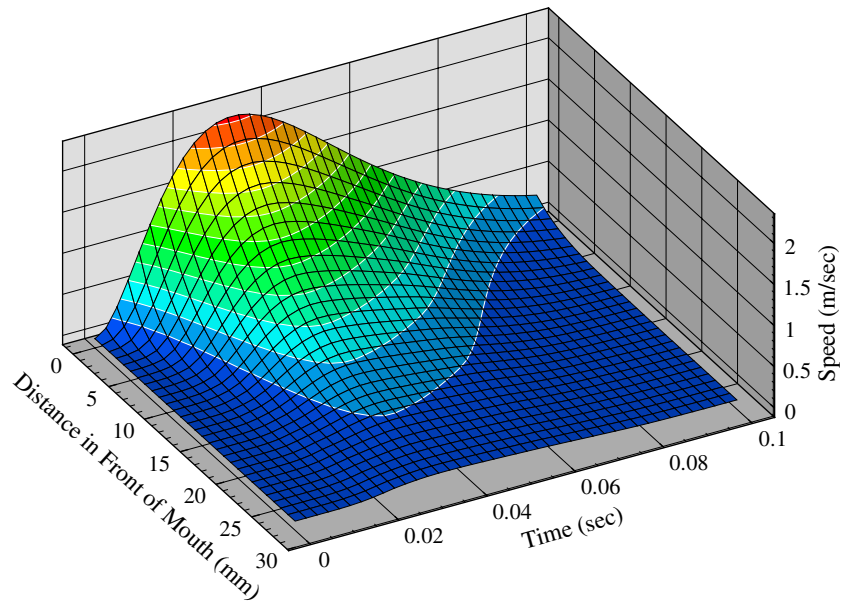


Fig. 7 The symbols show measured pressures within the mouth and in front of the fish. The dashed lines show predictions of pressure at the mouth aperture calculated by applying Eq 3 to the time sequence of measured speeds along the centerline

Fluid speed was not constant during the course of the feeding event, increasing from zero to peak fluid speed in  $40 \pm 18$  ms. The time of peak fluid speed occurred near the onset of peak gape ( $38 \pm 21$  ms). The synchronization of fluid speed and gape is potentially a very effective feeding strategy because the fish simultaneously maximizes both the steady and unsteady models, plotted versus the measured peak induced forces acting on the prey and the space over which pressure

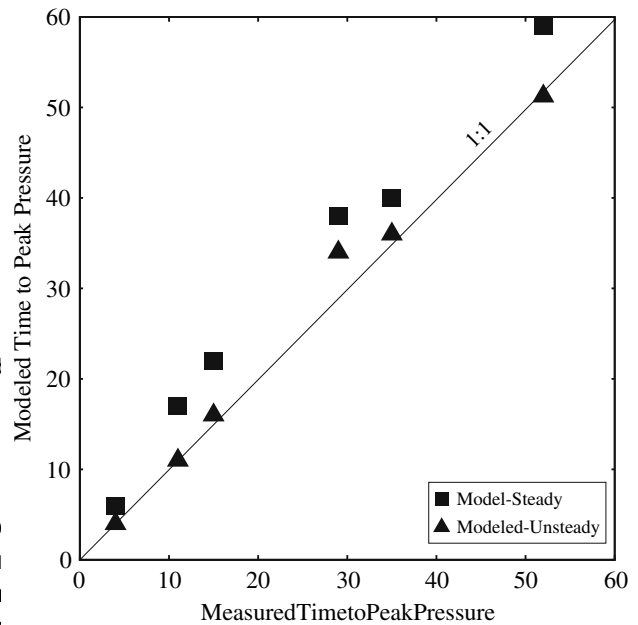


Fig. 8 Comparison of the time to peak pressure, as predicted by both the steady and unsteady models, plotted versus the measured peak induced forces acting on the prey and the space over which pressure

continued expansion of the posterior portion of the buccal cavity (Lauder 1982). The second is that the opening of the anterior opercular slits allows fluid to continue to flow into and through the mouth, driven only by fluid momentum, after total mouth past peak gape. A distinct delay in the posterior volumetric expansion of the buccal cavity has ceased. At the beginning of the feeding, when the opercular slits are abduction) relative to gape was shown consistently throughout feedings of three species of centrarchid fish exactly equal to the instantaneous volumetric expansion of the anterior opercular slits are open, the flow into the mouth is equal to any remaining expansion of the mouth cavity in addition to

the volumetric flow rate out of the opercular slits. After the demonstrated the latter. Our measurements demonstrate mouth has reached full expansion, the velocity of the fluid that the pressure at the mouth aperture is very nearly the cannot continue to increase. However, the flow will continue as at the posterior location of the mouth for all times after time on its own momentum, slowing due to losses, while the onset of peak gape, which is perhaps one reason why the mouth is held open. It is likely that both the anterior-to-posterior prediction of the pressure at the mouth aperture agrees with the posterior expansion and timing of opercular opening consistent with the measured pressure.

Although the predictions of the timing of peak pressure agree well with observations, the magnitude of estimated velocity is always lower than observed. This could be due to radial movement of the mouth walls resulting in streamline curvature, losses at the mouth opening, or viscous losses both within and outside the mouth, none of which are accounted for in the integration of one-dimensional form of the momentum equation given in Eq. 1.

Although a relationship between the velocity and pressure was always lower than observed. This could be due to radial movement of the mouth walls resulting in streamline curvature, losses at the mouth opening, or viscous losses both within and outside the mouth, none of which are accounted for in the integration of one-dimensional form of the momentum equation given in Eq. 1. As a result of statements to this effect and support from numerical models that show that the magnitude of generated buccal pressure is very sensitive to the shape of the mouth cavity, the mouth aperture is on the order of 50 gs and even higher in some species, such as the bluegill, as was shown in Day et al. (2005). Both the spatial gradients of velocity and acceleration contribute to pressure gradient within the flow field, which Wainwright and Day (2007) have shown exerts substantial forces on the prey. This study represents a significant advance in understanding the relationship between pressure and velocity in this dynamic fluid flow because it measures both simultaneously and demonstrates good temporal agreement between the fluid velocity speed is correlated to the magnitude of peak suction pressure. In addition to the intra-oral pressure, this

This study quantifies the degree to which the time course of buccal pressure is affected by the unsteady nature of the flow. When the unsteady terms are included in the relationship between the velocity field and pressure, the prediction of pressure at the mouth leads to excellent temporal agreement with the measured buccal pressure. Exclusion of these terms (a quasi-steady assumption) leads to a slightly lower magnitude and temporal latency of the prediction. In conclusion, we find that the equations of motion can, in fact, be used to relate pressure measured inside the mouth cavity, to the flow field outside the mouth, at least up until the time when the opercula are opened at the back of the head. This is the first such demonstration for suction feeding fishes and establishes an important physical link between the pressures that are generated during expansion of the head and the flow that results and is used to capture prey. Our understanding of the fluid mechanics of suction feeding has advanced considerably in recent years, but as yet there has not been a detailed treatment of the mechanics of internal expansion of the oral cavity and how this pattern relates to flow entering the mouth. These results are an important step in this direction that will lead to a greater understanding of how internal head movements can be regulated to control flow in front of the fish.

In this study we have demonstrated that in at least one species of fish, there is a clear relationship between pressure within the mouth and fluid speed outside the head. We propose that because of properties and characterization of the flow field, measured pressures within the mouth could, in fact, be used to derive the flow outside the fish. This is primarily due to the fact that there is a general function for the velocity distribution in front of the fish that is valid for all times during the feeding and over a wide range of behavioral variations, as was shown in Day et al. (2005) and Higham et al. (2006). By accounting for only two variables, i.e. mouth size and fluid speed at the mouth, we can characterize velocity in front of the fish. Assuming that mouth size is known as a function of time, the pressure at the mouth aperture can be used to predict the velocity at the mouth aperture or vice versa. In this study, we have

**Acknowledgments** This research was supported by NSF grants IOB-0444554 and 0610310.

## References

- Adrian RJ (1991) Particle imaging techniques for fluid mechanics. *Annu Rev Fluid Mech* 23:261–304
- Adrian RJ (1997) Dynamic ranges and spatial resolution of particle image velocimetry. *Meas Sci Technol* 8:1393–1398
- Aerts P (1990) Variability of the fast suction feeding process in *Astatotilapia elegans* (Teleostei, Cichlidae): a hypothesis of peripheral feedback control. *J Zool* 220:653–678
- Aerts P, Osse JWM, Verraes W (1987) Model of jaw depression during feeding in *Astatotilapia elegans* (Teleostei, Cichlidae): mechanisms for energy-storage and triggering. *J Morphol* 194:85–109
- Batchelor GK (1967) An introduction to fluid mechanics. Cambridge University Press, Cambridge
- Carroll AM, Wainwright PC, Huskey SH, Collar DC, Turnigan RG (2004) Morphology predicts suction feeding performance in centrarchid fishes. *J Exp Biol* 207:3873–3881
- Day SW, Higham TE, Cheer AY, Wainwright PC (2005) Spatial and temporal patterns of water flow generated by suction-feeding bluegill sunfish *Lepomis macrochirus* resolved by particle image velocimetry. *J Exp Biol* 208:2661–2671
- Drost MR, Muller M, Osse JWM (1988) A quantitative hydrodynamical model of suction feeding in larval fishes: the role of frictional forces. *Proc R Soc Lond Ser B* 234:263–281
- Durrani TS, Greated CA (1977) Laser systems in flow measurements. New York: Wiley
- Ferry-Graham LA, Wainwright PC, Lauder GV (2003) Quantification of flow during suction feeding in bluegill sunfish. *Zoology* 106:159–168
- Higham TE, Day SW, Wainwright PC (2005) Sucking while swimming: evaluating the effects of ram speed on suction generation in bluegill sunfish *Lepomis macrochirus* using digital particle image velocimetry. *J Exp Biol* 208:2653–2660
- Higham TE, Day SW, Wainwright PC (2006a) Multidimensional analysis of suction feeding performance in fishes: fluid speed, acceleration, feeding accuracy and the ingested volume of water. *J Exp Biol* 209:2713–2725
- Higham TE, Day SW, Wainwright PC (2006b) The pressures of suction feeding: the relation between buccal pressure and induced fluid speed in centrarchid fishes. *J Exp Biol* 209:3281–3287
- Higham TE, Hulsey CD, Rican O, Carroll AM (2007) Feeding with speed: prey capture evolution in cichlids. *J Evol Biol* 20:70–78
- Lauder GV (1980) The suction feeding mechanism in sunfishes (Lepomidae): an experimental analysis. *J Exp Biol* 88:49–72
- Lauder GV (1982) Patterns of evolution in the feeding mechanism of actinopterygian fishes. *Am Zool* 22:275–285
- Lauder GV, Clark BD (1984) Water flow patterns during prey capture by teleost fishes. *J Exp Biol* 113:143–150
- Liem KF (1973) Modulatory multiplicity in the feeding mechanism in cichlid fishes, as exemplified by the invertebrate pickers of Lake Tanganyika. *J Zool Soc Lond*, pp 93–125
- Muller M, Osse JWM (1984) Hydrodynamics of suction feeding fish. *Trans Zool Soc Lond* 37:51–135
- Muller M, Osse JWM, Verhagen JHG (1982) A quantitative hydrodynamical model of suction feeding in fish. *J Theor Biol* 95:49–79
- Nauwelaerts S, Wilga C, Sanford C, Lauder G (2007) Hydrodynamics of prey capture in sharks: effects of substrate. *J R Soc Interface* 4(13):341–345
- Nemeth DH (1997) Modulation of buccal pressure during prey capture in *Hexagrammos decagrammus* (Teleostei: Hexagrammidae). *J Exp Biol* 200:2145–2154
- Norton SF (1991) Capture success and diet of cottid fishes: the role of predator morphology and attack kinematics. *Ecology* 72:1807–1819
- Norton SF, Brainerd EL (1993) Convergence in the feeding mechanics of ecomorphologically similar species in the Centrarchidae and Cichlidae. *J Exp Biol* 176:11–29
- Nyberg DW (1971) Prey capture in largemouth bass. *Am Midl Nat* 86:128–144
- Sanford CPJ, Wainwright PC (2002) Use of sonomicrometry demonstrates the link between prey capture kinematics and suction pressure in largemouth bass. *J Exp Biol* 205:3445–3457
- Scarano F, Reithmuller ML (1999) Iterative multigrid approach in PIV image processing with discrete window offset. *Exp Fluids* 26:513–523
- Svanback R, Wainwright PC, Ferry-Graham LA (2002) Linking cranial kinematics, buccal pressure, and suction feeding performance in largemouth bass. *Physiol Biochem Zool* 75:532–543
- van Leeuwen JL, Muller M (1983) The recording and interpretation of pressures in prey-sucking fish. *Neth J Zool* 33:425–475
- van Leeuwen JL, Muller M (1984a) A quantitative study of flow in prey capture by rainbow trout *Salmo gairdneri* with general consideration of the actinopterygian feeding mechanism. *Trans Zool Soc Lond* 37:171–227
- van Leeuwen JL, Muller M (1984b) Optimum sucking techniques for predatory fish. *Trans Zool Soc Lond* 37:137–169
- van Wassenbergh S, Aerts P, Herrel A (2006) Hydrodynamic modelling of aquatic suction performance and intra-oral pressures: limitations for comparative studies. *J R Soc Interface* 3:507–514
- Wainwright PC, Day SW (2007) The forces exerted by aquatic suction feeders on their prey. *J R Soc Interface* 4:553–560
- Wainwright PC, Huskey SH, Turingan RG, Carroll AM (2006) Ontogeny of suction feeding capacity in snook *Centropomus undecimalis*. *J Exp Zool A* 305A:246–252
- Weihs D (1980) Hydrodynamics of suction feeding fish in motion. *J Fish Biol* 16:425–433